This pdf file consists of all pages containing figures within:

A multi-proxy study of planktonic foraminifera to identify past millennial-scale climate variability in the East Asian Monsoon and the Western Pacific Warm Pool

by

Stefanie Dannenmann

A Dissertation

Submitted to the University at Albany, State University of New York

in Partial Fulfillment for the degree of

Doctor of Philosophy

College of Arts & Sciences

Department of Earth and Atmospheric Sciences

2001

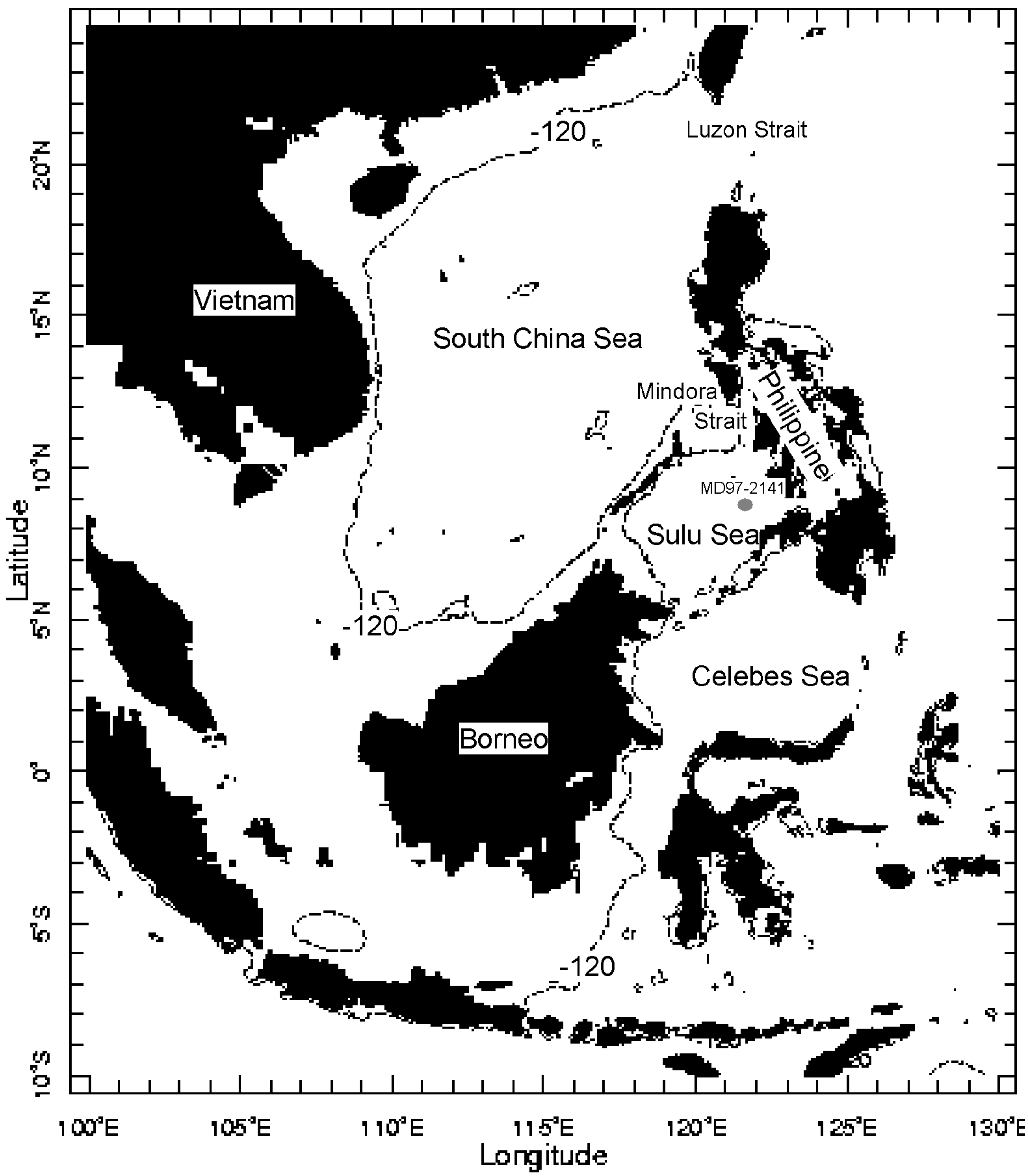

Figure 1.1: Map of western tropical Pacific showing the location of Sulu Sea. Bathymetric contour is the 120 m isobath indicating the approximate position of coast line during glacial maximum low sea level stand. A gray circle indicates location of IMAGES site MD97-2141.

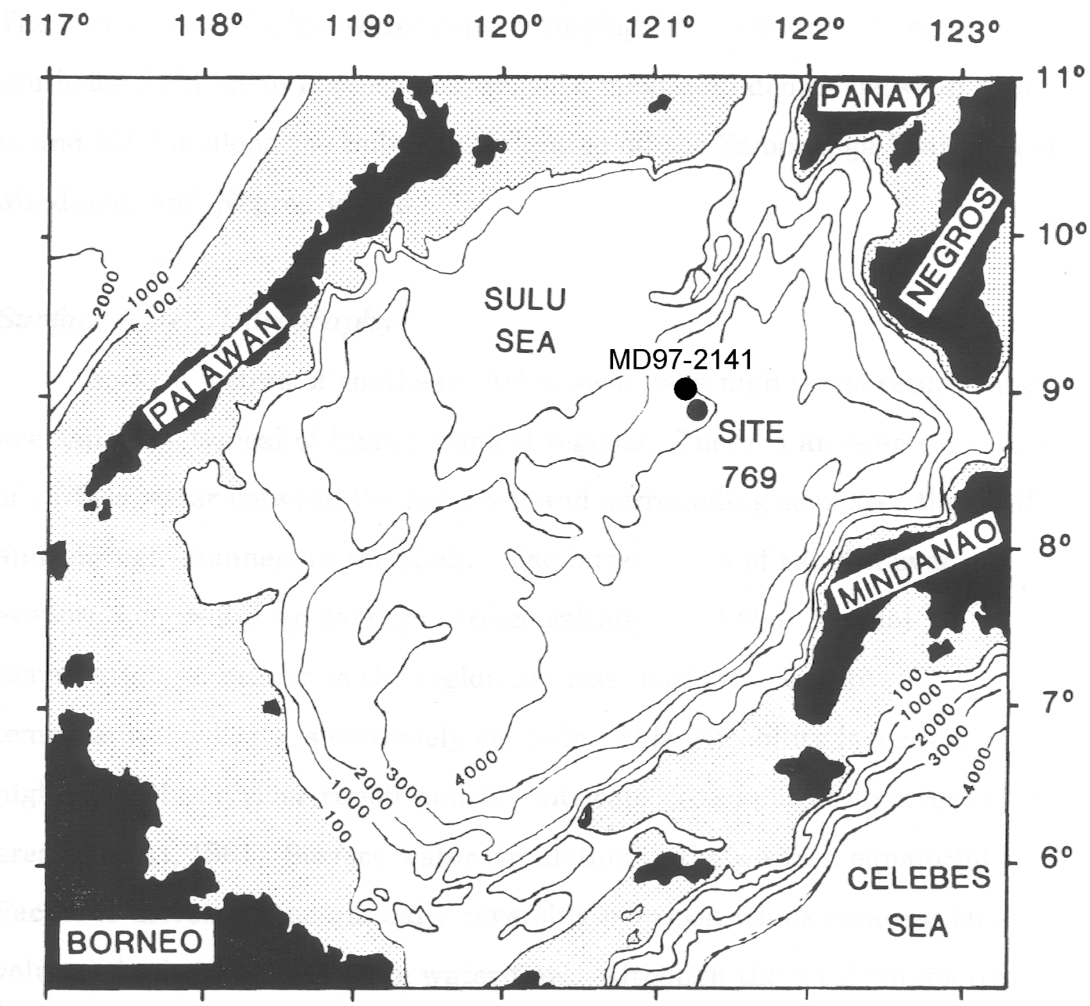

Figure 1.2: Detailed bathymetric map of the Sulu Sea. Bathymetric contour is presented in meters. Shelf shallower than 100 meter is marked by the shaded zone. Location of IMAGES site MD97-2141 (3,633 m) and ODP site 769A (3,643 m) are indicated by black circles.

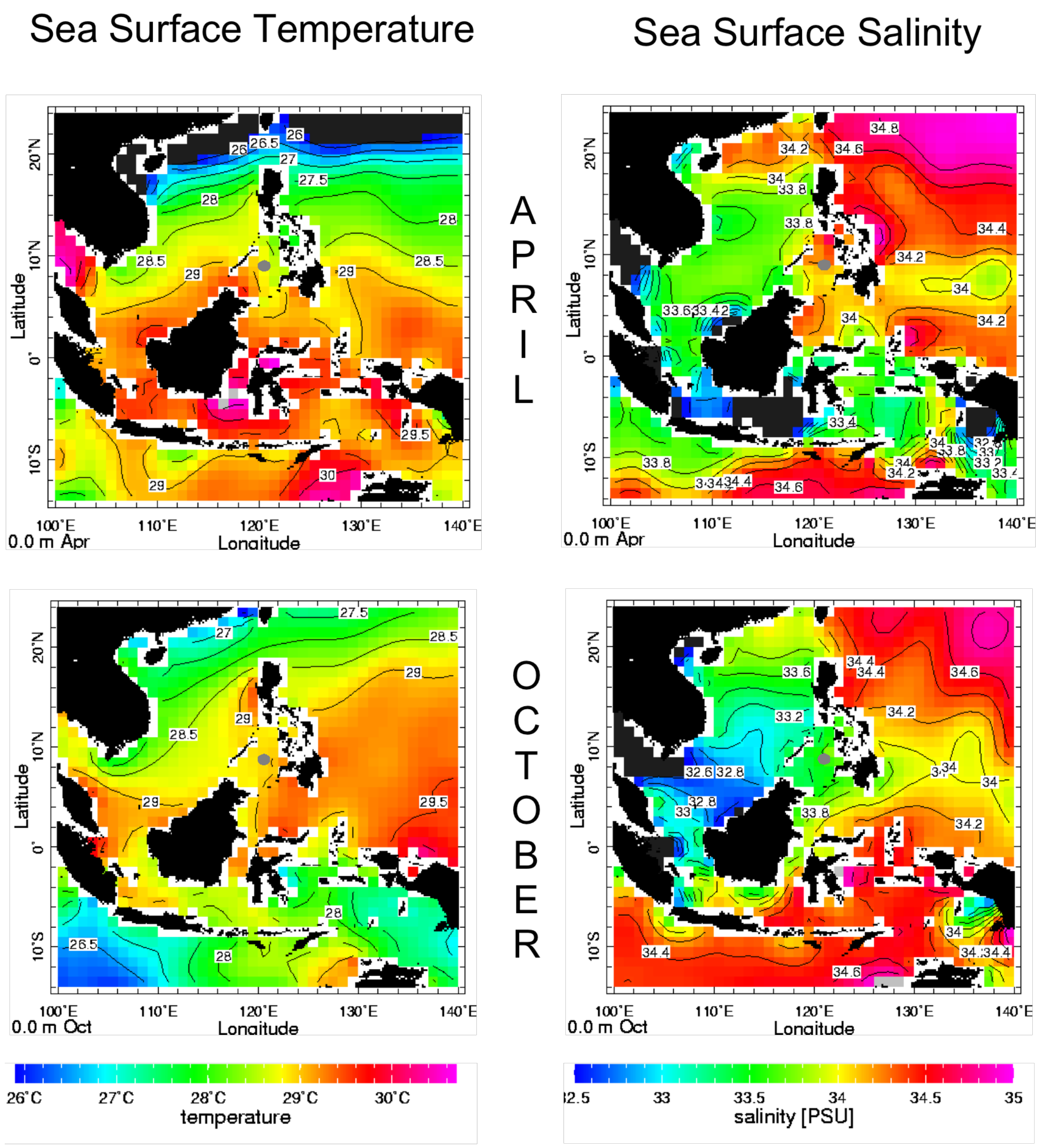

M. Conkright, et al., World Ocean Atlas 1998 CD-ROM Data Set

Figure 1.3: Average sea surface temperature and sea surface salinity in Indonesia and the western Pacific for the end of the winter monsoon (April) and the end of summer monsoon (October), highlighting maximal seasonal monsoon changes in surface conditions. Note the location of IMAGES core MD97-2141 that is marked by a gray circle. In the Sulu Sea the influence of East Asian Monsoon-driven river runoff and precipitation in Borneo and coastal regions of the mainland is evident as is the influence of the western Pacific on surface salinity [Data from *Conkright et al.*, 1998].

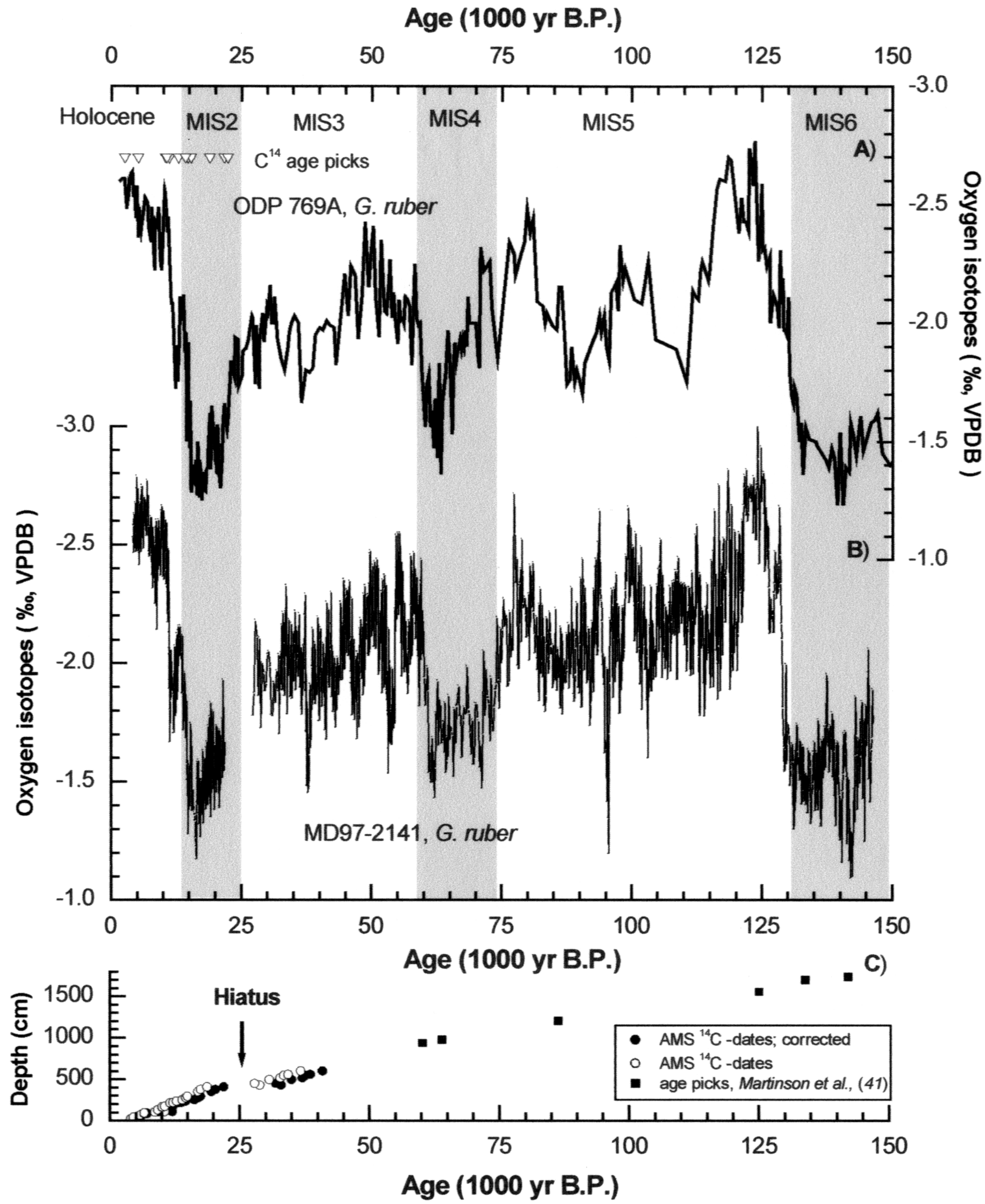

Figure 2.1: (A) Sulu Sea δ^{18}O record of *G. ruber* ($\delta^{18}O_{G.\ ruber}$) from ODP Site 769A (upper solid black line) [*Linsley*, 1996] with open down triangles indicating ^{14}C for this site, and from IMAGES core MD97-2141 (lower thin solid line) [this study]. Note that no attempt has been made to temporally align the ODP 769A and MD97-2141 δ^{18}O records. **(C)** Chronology for MD97-2141, consisting of 28 AMS radiocarbon age dates (solid black circles) and several correlation points with the *Martinson et al.* [1987] chronology (solid black squares).

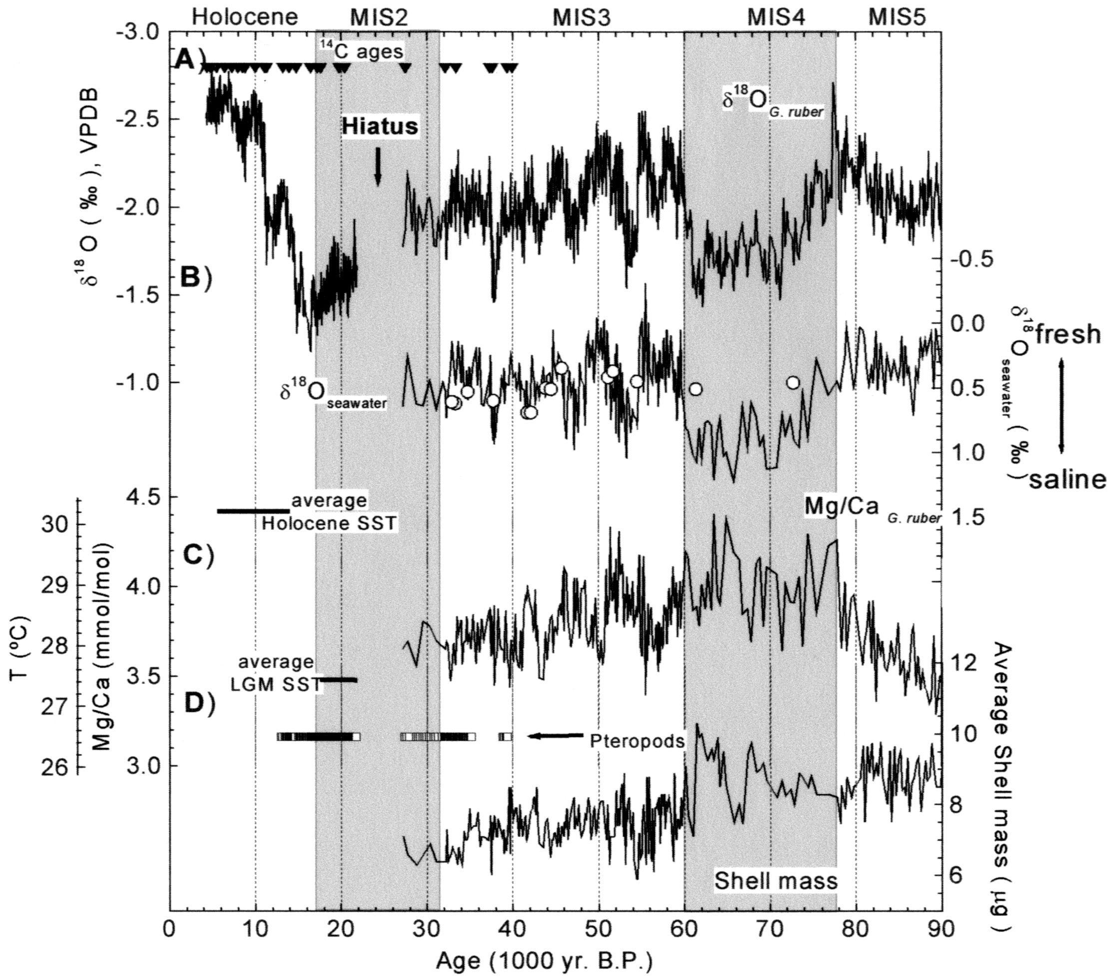

Figure 2.2: Data from the Sulu Sea during the last 90 kyr. Grey shaded areas represent marine isotope stages 2 and 4. **(A)** Sulu Sea $\delta^{18}O_{G. ruber}$; black down triangles indicate ^{14}C ages. **(B)** Sulu Sea $\delta^{18}O_{seawater}$; $\delta^{18}O_{seawater}$ has been calculated using the empirically derived temperature : $\delta^{18}O$ relationship based on planktonic foraminifera generated by *Erez & Luz* [1983] and the Mg/Ca –SST relationship reported by *Lea et al*. [2000]. Superimposed are sea level data (open circle) measured by *Fairbanks* [1989] and *Chappell et al*., [1996] **(C)** Sulu Sea Mg/Ca *G. ruber*; temperature estimates are calculated using *Lea et al.* [2000] equation. Horizontal lines indicate average Mg/Ca composition during Holocene and LGM [*from Rosenthal et al*., 2000a]. **(D)** Average shell mass in µg.

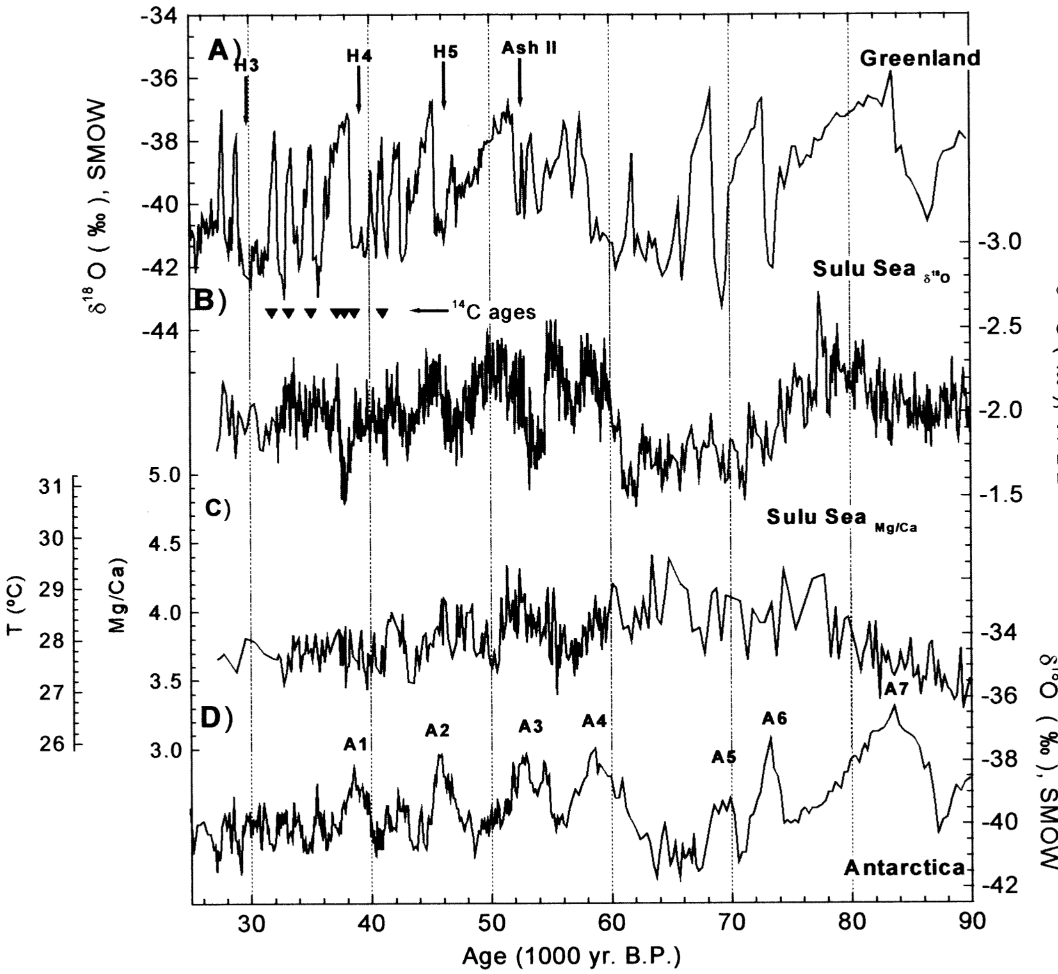

Figure 2.3: Comparison of the isotopic records from Greenland and Antarctica to isotopic and trace element data from the Sulu Sea between 27,000 and 90,000 years. The Greenland and Antarctica time scales between 25-90 kyr are based on correlating atmospheric methane records from these cores [*Blunier and Brooks*, 2001]. Sulu Sea data are on an independent time scale. **(A)** Greenland Ice core (GISP2) $\delta^{18}O$ data [*Blunier and Brooks,* 2001]. Occurrence of Heinrich events are indicated by H3-H5. **(B)** Sulu Sea $\delta^{18}O_{G.\ ruber}$; black triangles indicate ^{14}C ages. **(C)** Sulu Sea Mg/Ca$_{G.\ ruber}$; temperature estimates are calculated using *Lea et al.* [2000] equation. **(D)** Antarctica $\delta^{18}O$ data [*Blunier and Brooks,* 2001]. Antarctic warming events are indicated by A1-A7.

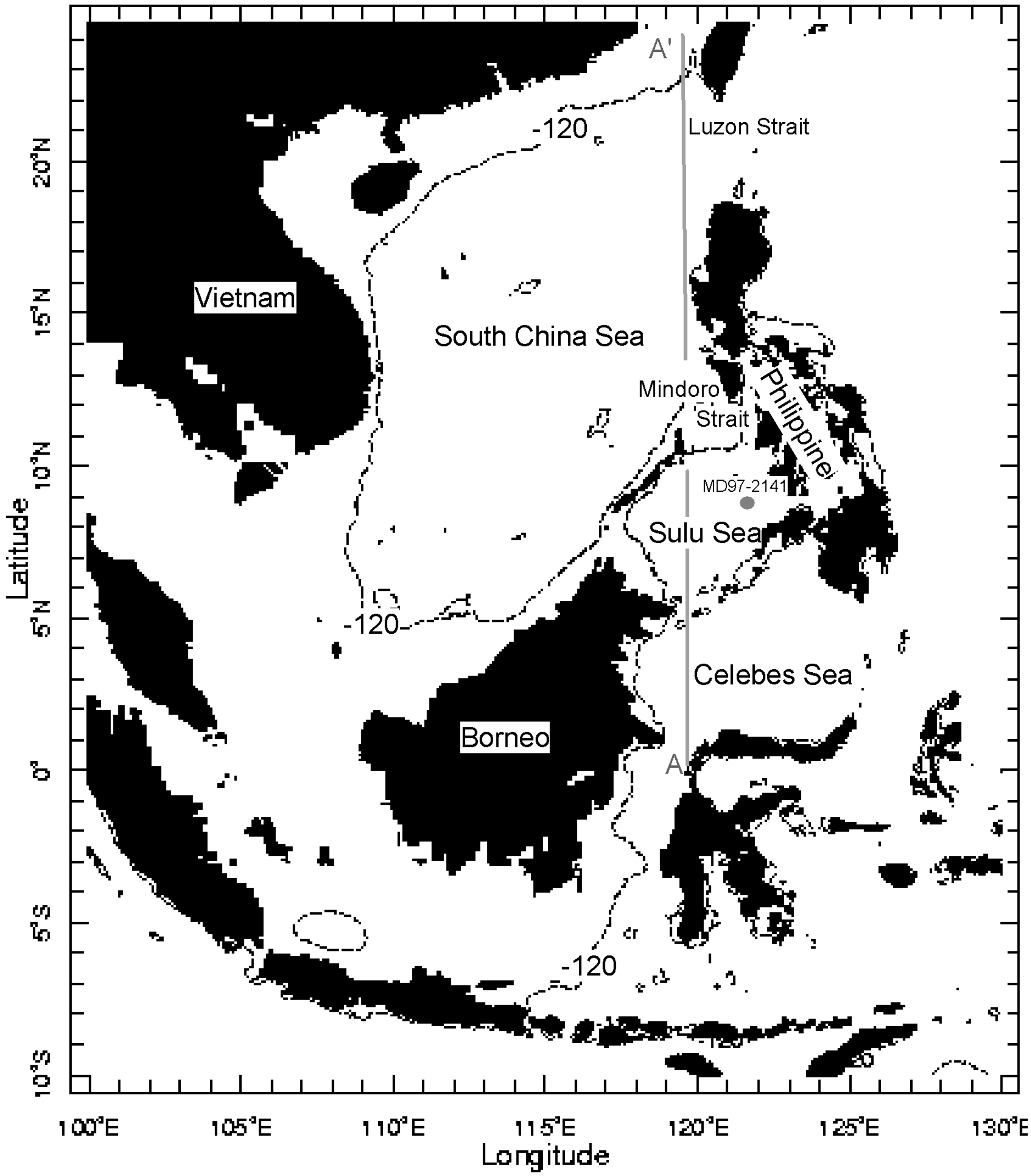

Figure 3.1: Map of western tropical Pacific showing location of the Sulu Sea and the location of IMAGES core MD97-2141 (gray circle). Bathymetric contour is the 120 m isobath indicating the approximate position of coast line during glacial maximum low sea level stand. A - A' cross section illustrated in **Figure 3.2**.

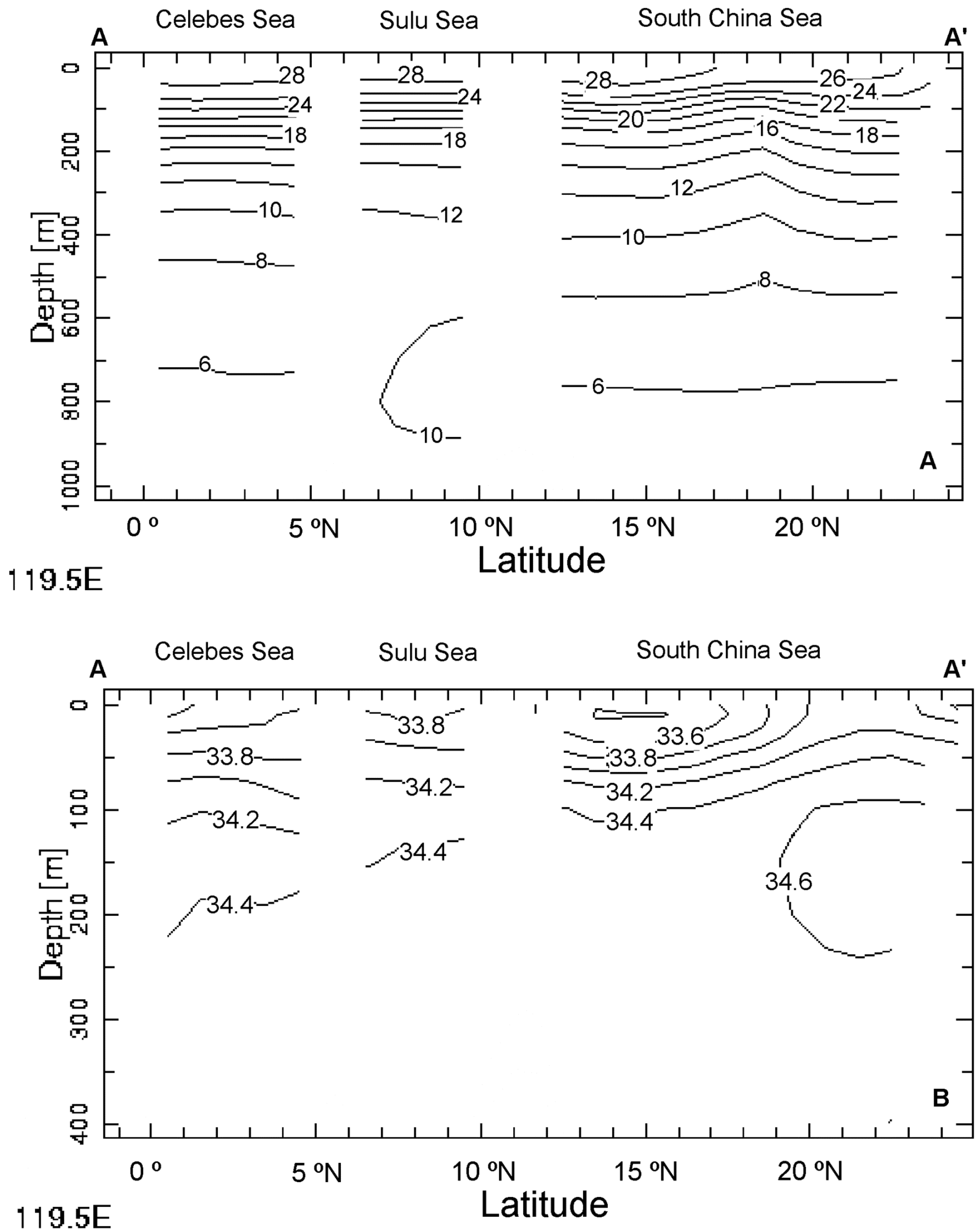

Figure 3.2: Vertical profiles of annual averaged **(A)** temperature (upper 1000m) and **(B)** salinity (upper 400m) along north-south line A-A' shown in Figure 3.1 (119.5º E) [Data from *Conkright et al*., 1998]. Note the warm (10°C) bottom waters in the Sulu Sea.

G. tumida because it is more abundant, and it calcifies at approximately 200 m water depth, the depth where high salinity water intrudes into the Sulu Sea through the Mindoro Strait. Therefore it is possible to monitor the influence of the NPTW during MIS3. Information about calcification depth, calcification temperature, temperature and salinity tolerance for each species is summarized in Table 2.

Table 2. Summary of modern living habitat for *G. ruber*, *G. sacculifer*, *N. dutertrei*, and *G. crassaformis*

	G. ruber	***G. sacculifer***	***N. dutertrei***	***G. crassaformis***
calcification depth (meters)	< 25m	< 25m	125m	200 - 300 m
calcification temperature	~24°C	~26°C	15°C	10°C
temperature tolerance	16°C - 31°C	14°C - 31°C	13°C - 33°C	rarely been observed in the living state
salinity tolerance	22‰ - 49‰	24‰ - 47‰	25‰ - 46‰	-
Comments	mixed layer	mixed layer	thermocline	sub-thermocline

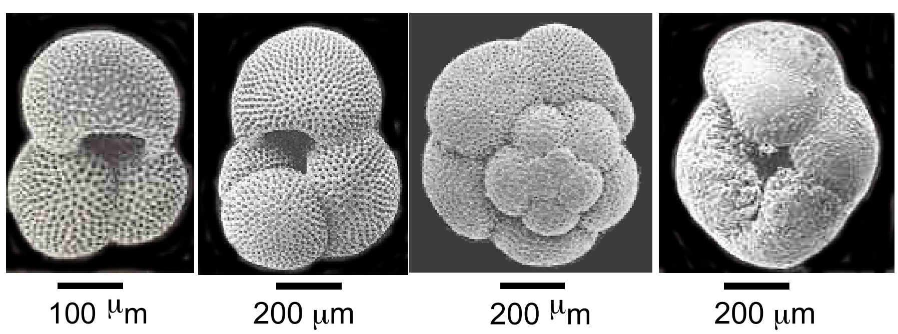

Hemleben et al [1989]

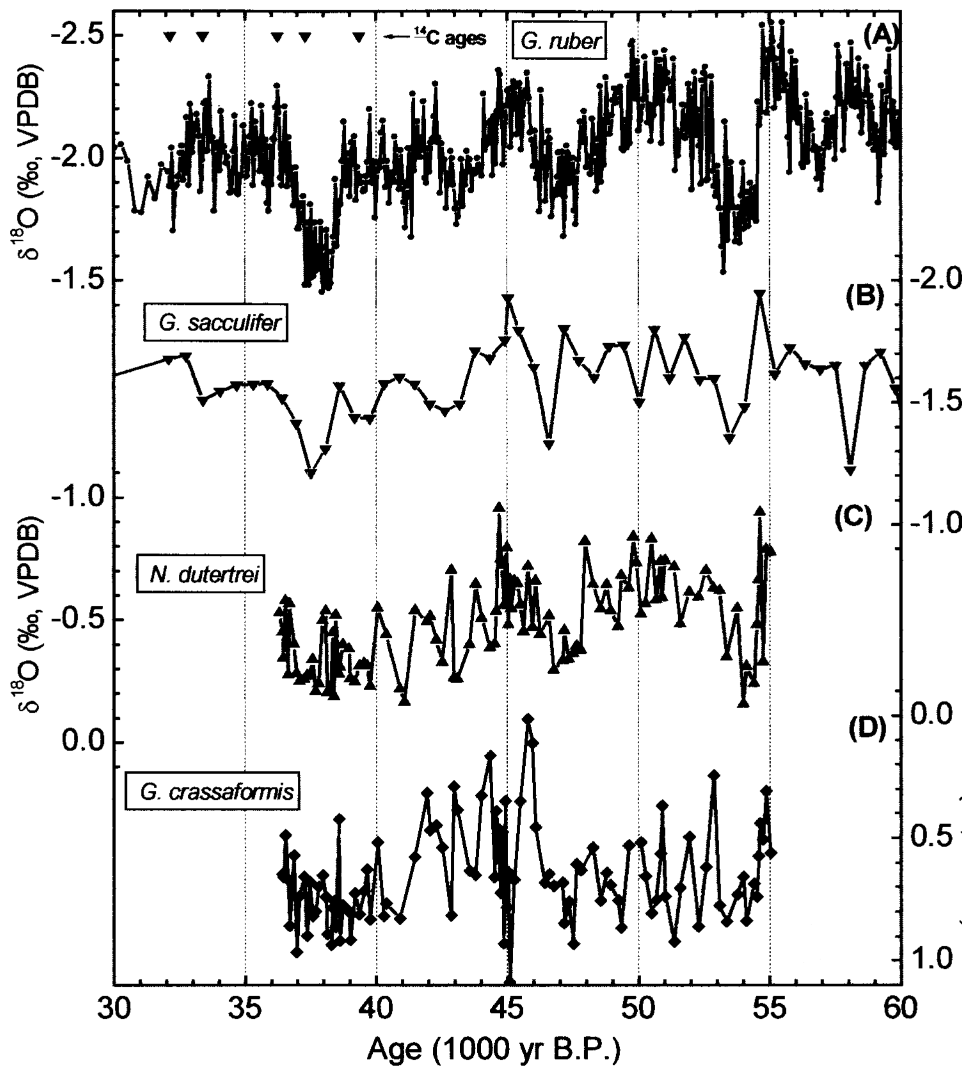

Figure 3.3: Planktonic foraminiferal $\delta^{18}O$ records plotted against time for each species analyzed in IMAGES core MD97-2141 during marine isotope stage 3. **(A)** *Globigerinoides ruber* (circles); black triangles indicate ^{14}C ages. **(B)** *Globigerinoides sacculifer* (down triangles) **(C)** *Neogloboquadrina dutertrei* (up triangles) **(D)** *Globorotalia crassaformis* (diamonds). Note that the y-axis scale range for all plots is 1.2 ‰.

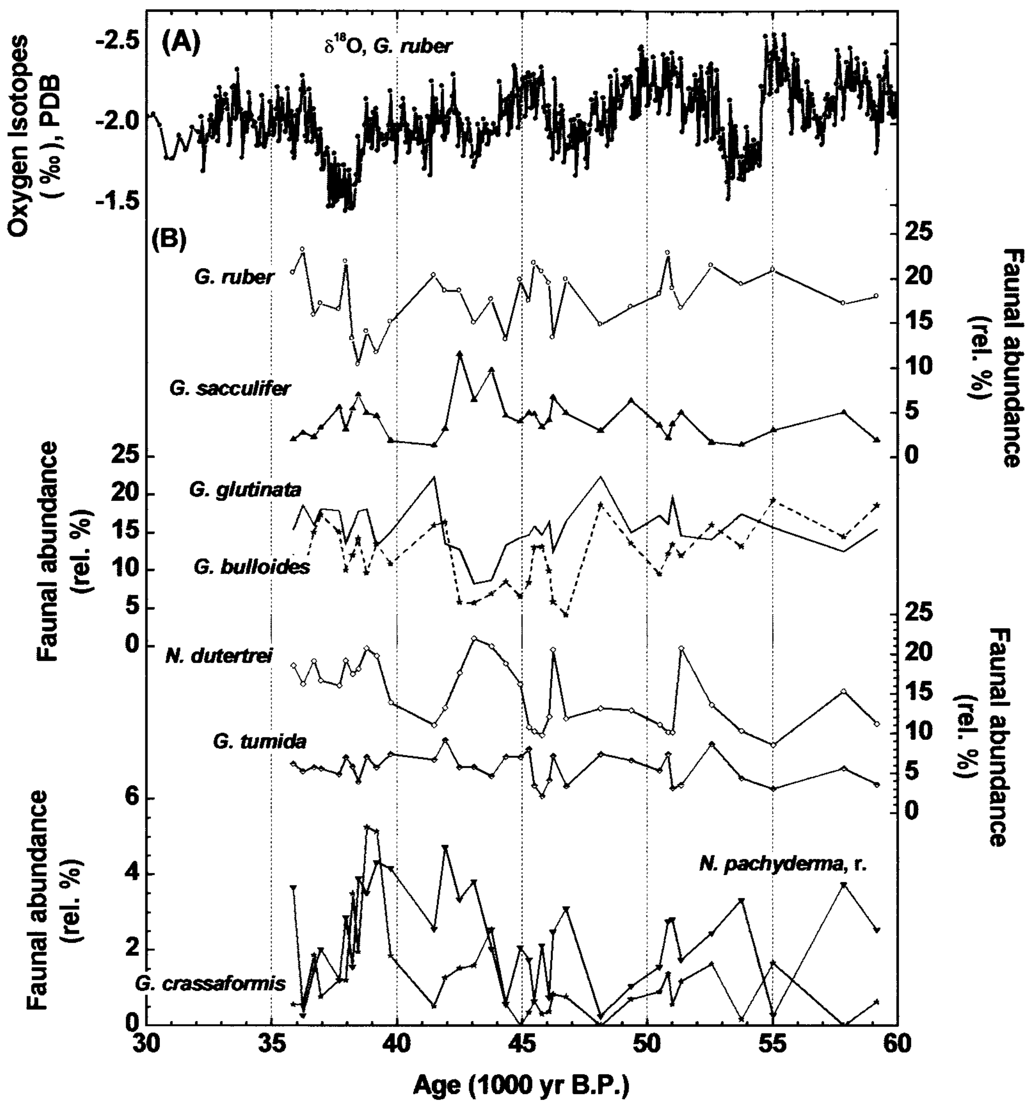

Figure 3.4: (A) The $\delta^{18}O$ values of planktonic *G. ruber* for MIS3. **(B):** Downcore variations in the percent relative abundance of 8 planktonic foraminifera species during MIS3 at MD97-2141. Four mixed-layer species: *G. ruber, G. sacculifer, G. glutinata, G. bulloides*; two thermocline species: *N. dutertrei, G. tumida*; and two sub-thermocline species: *N. pachyderma (r.)*, and *G. crassaformis.*

mixed layer species explain 73% variance of the data set (Table 4), and indicate greater variability between ~ 35-47 kyr (Figure 3.5). In contrast, "thermocline" species only explain 11% variance of faunal data, and display a mirror image to the mixed layer species (Figure 3.5). Changes from maxima to minima abundance for mixed layer and thermocline species vary from 5-15 % and 10-15 %, respectively. Overall, the changes in the thermocline species are larger for a single event compared to changes in the mixed layer species.

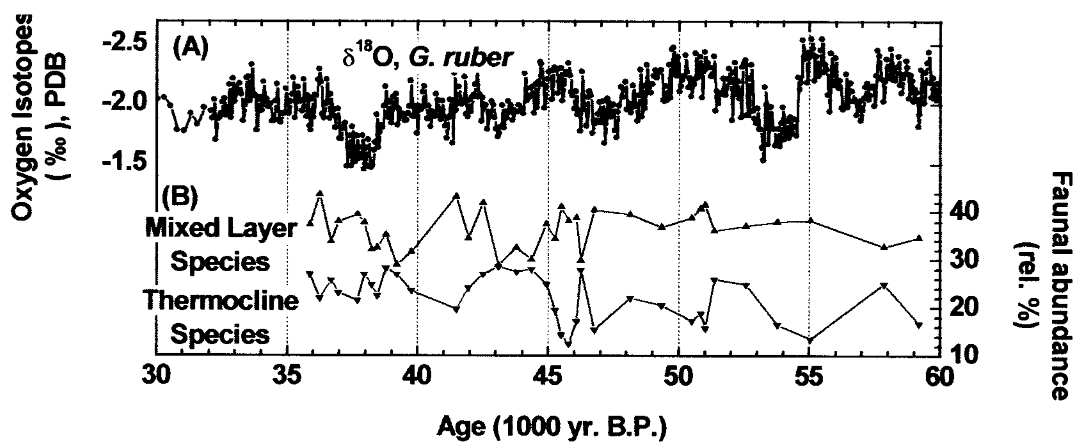

Figure 3.5: (A) $\delta^{18}O_{G.\ ruber}$ during MIS3. **(B):** Time series of the relative abundance sums of “mixed-layer” species *Globigerinoides ruber, Globigerinita glutinata, Globigerinoides sacculifer* and the relative abundance sum of “thermocline” dwellers *Globorotalia menardii, Pulleniatina obliquiloculata, Neogloboquadrina dutertrei, and Globorotalia tumida.*

How much of the observed changes in the $\delta^{18}O$ of the mixed layer dwellers can be explained by changes in the thermocline and sub-thermocline? To address this question *Chaisson and Ravelo* [1997] introduced the strategy to record and the overall trend of the thermocline abundance record between 40-50 kyr seem to correlate well with the magnetic susceptibility peaks (Figure 3.7). This indicates increased East Asian summer monsoon conditions, and therefore reduced influenced of the NPTW.

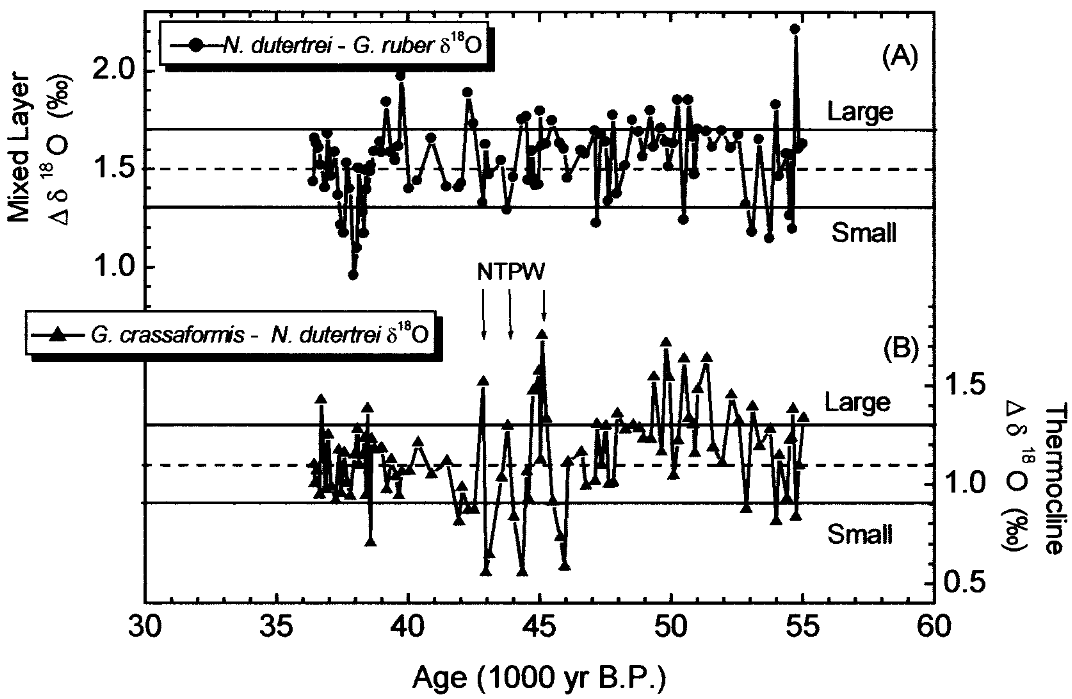

Figure 3.6: Oxygen isotope "difference" curves. **(A)** *Neogloboquadrina dutertrei* $\delta^{18}O$ - *Globigerinoides ruber* $\delta^{18}O$. **(B)** *Globorotalia Crassaformis* $\delta^{18}O$ - *Neogloboquadrina dutertrei* $\delta^{18}O$. Dashed horizontal lines represent average values. Solid lines represent average standard deviation. Possible influence of North Pacific Tropical Water (NPTW) is indicated by arrows.

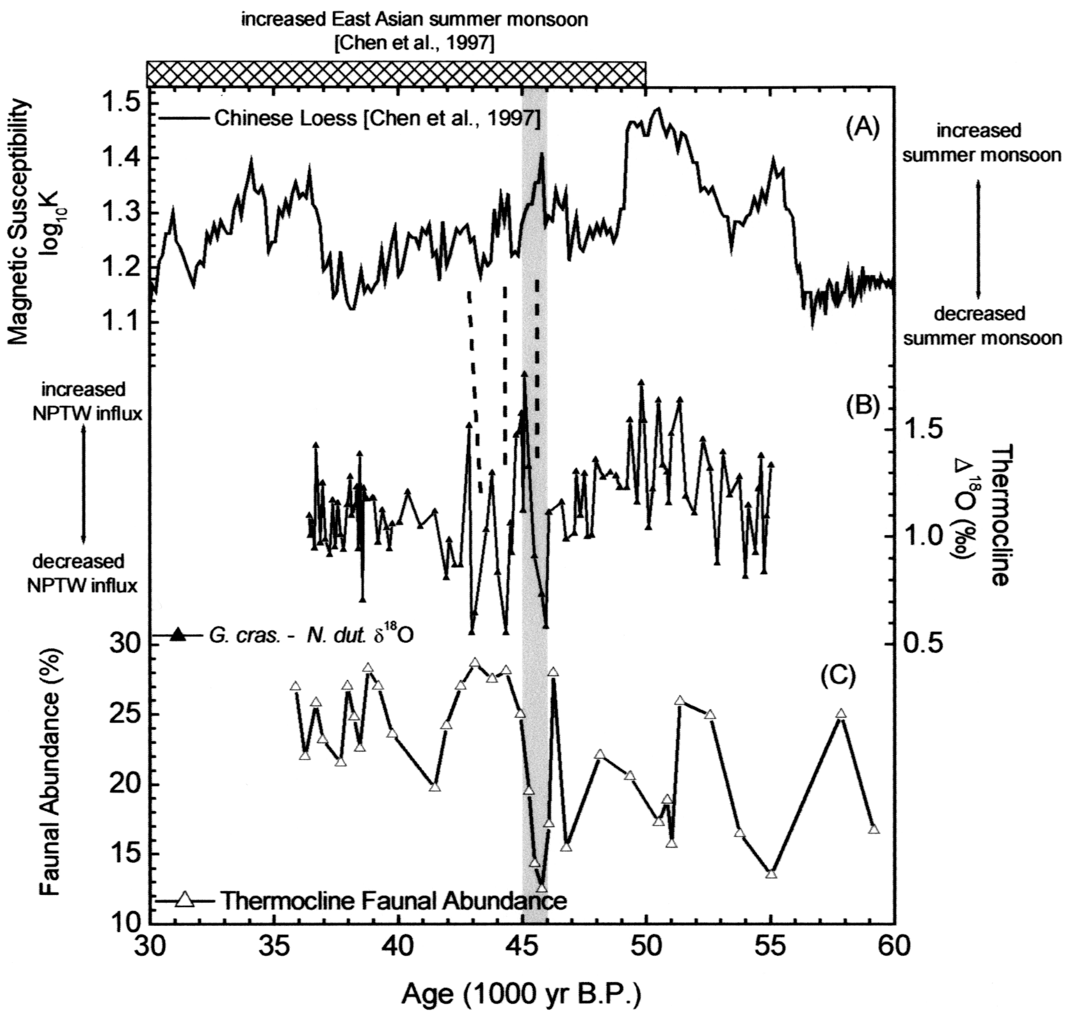

Figure 3.7: Comparison between Chinese loess and Sulu Sea data. **(A)** Chinese loess magnetic susceptibility data used as an index for East Asian monsoon activity [*Chen et al.*, 1997]. **(B)** Same figure as in Figure 3.6B. Dashed vertical lines represent possible correlation between the Chinese loess and Sulu Sea record during enhanced East Asian summer monsoon peaks. (C) Time series of the relative abundance sums of "thermocline" dwellers. *G. menardii, P. obliquiloculata, N. dutertrei, and G. tumida*. Greyshaded area indicates one example of a possible correlation of all three data sets between 45 and 46 kyr (see also Figure 3.5B).

[e.g., *Schneider et al*., 1996; *Rühlemann et al*., 1999; *Wang et al*., 1999; *Kudrass et al*., 2001].

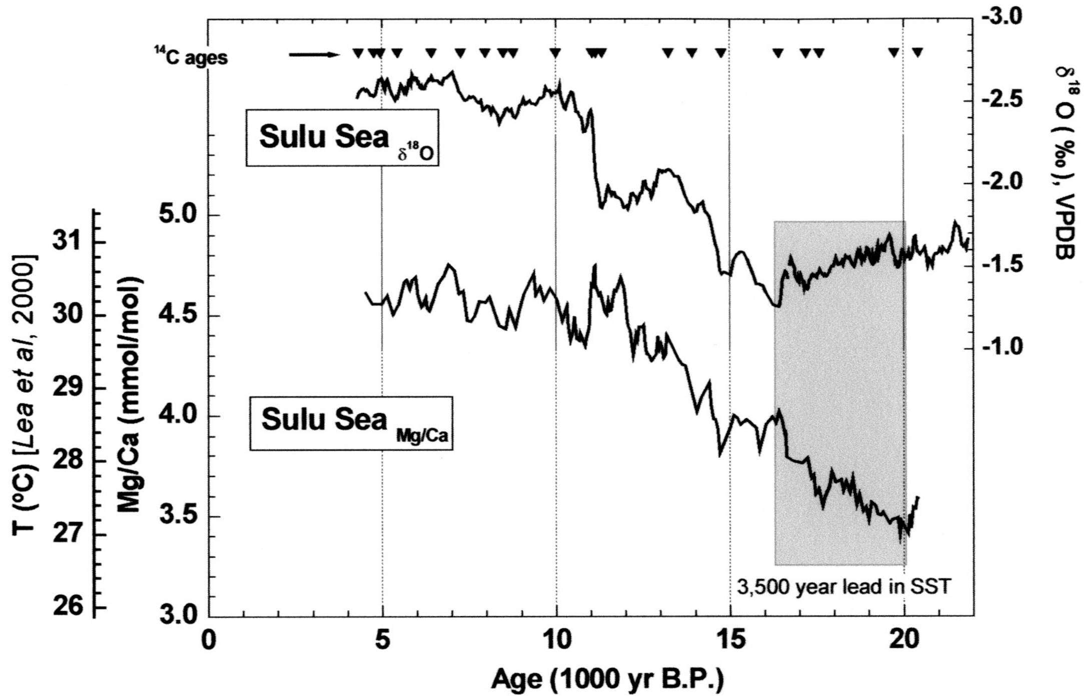

Figure 4.1: $\delta^{18}O$ and SST estimates based on Mg/Ca in the Sulu Sea for the last 21,000 years. This figure is used as an example to demonstrate the 3,500 year lead in SST between 17 and 20 kyr (Last Glacial Maximum). The data are smoothed with a 5 point running average. Down triangles indicate radiocarbon ages for this site. [Data from Chapter 2 and *Rosenthal et al.*, in prep].

This study examines in greater detail the relationship between inferred temperature changes and foraminiferal planktonic $\delta^{18}O$ in tropical oceans during the LGM and across the transition to the Holocene. Published reconstruction of SST and $\delta^{18}O$ data collected within the same sediment cores in mainly tropical

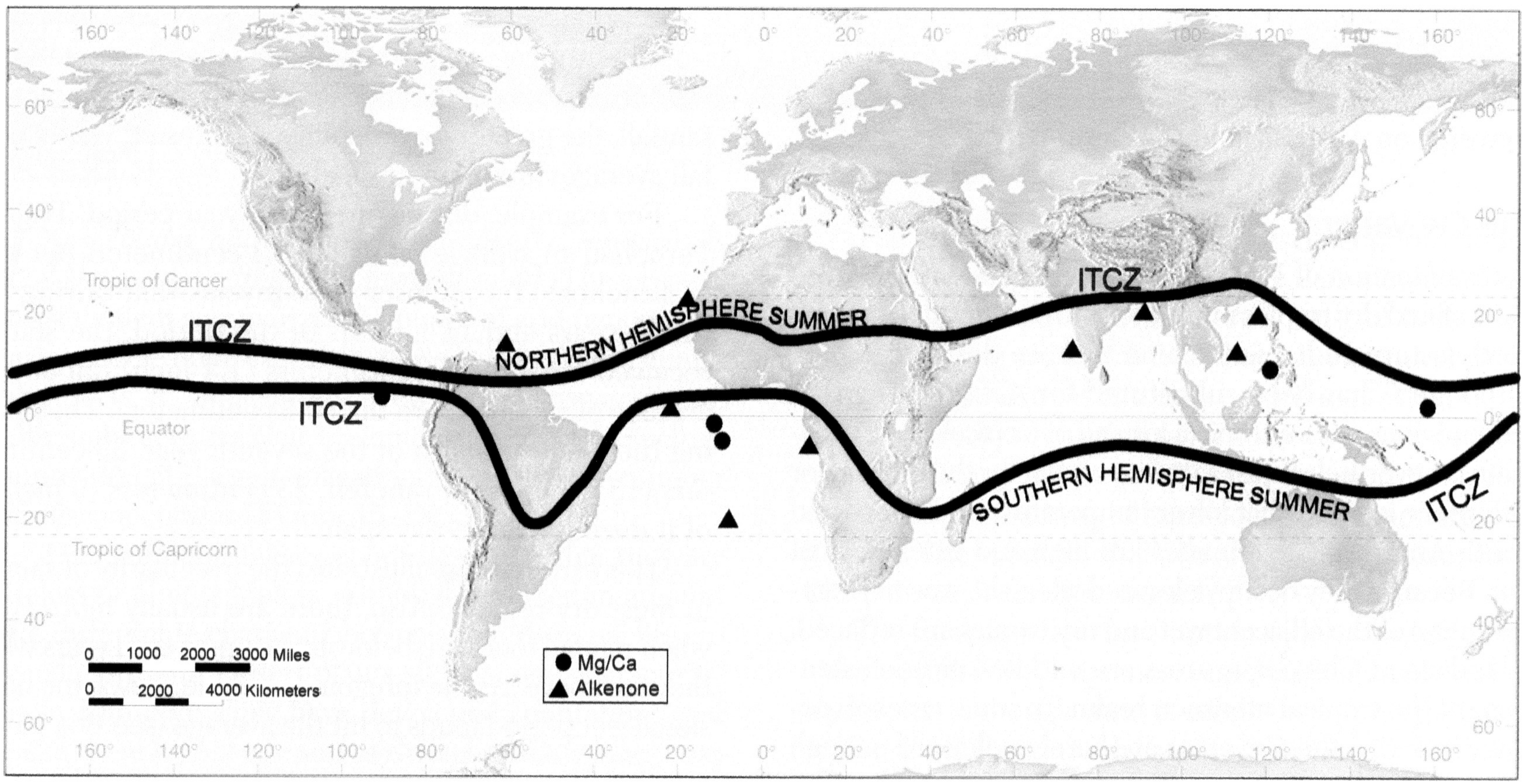

Figure 4.2: Location of ocean sediment cores used to examine glacial-interglacial sea surface temperature and salinity changes by means of Mg/Ca (circle) and alkenones (triangle) analyses. See Table 4 for location details and references.

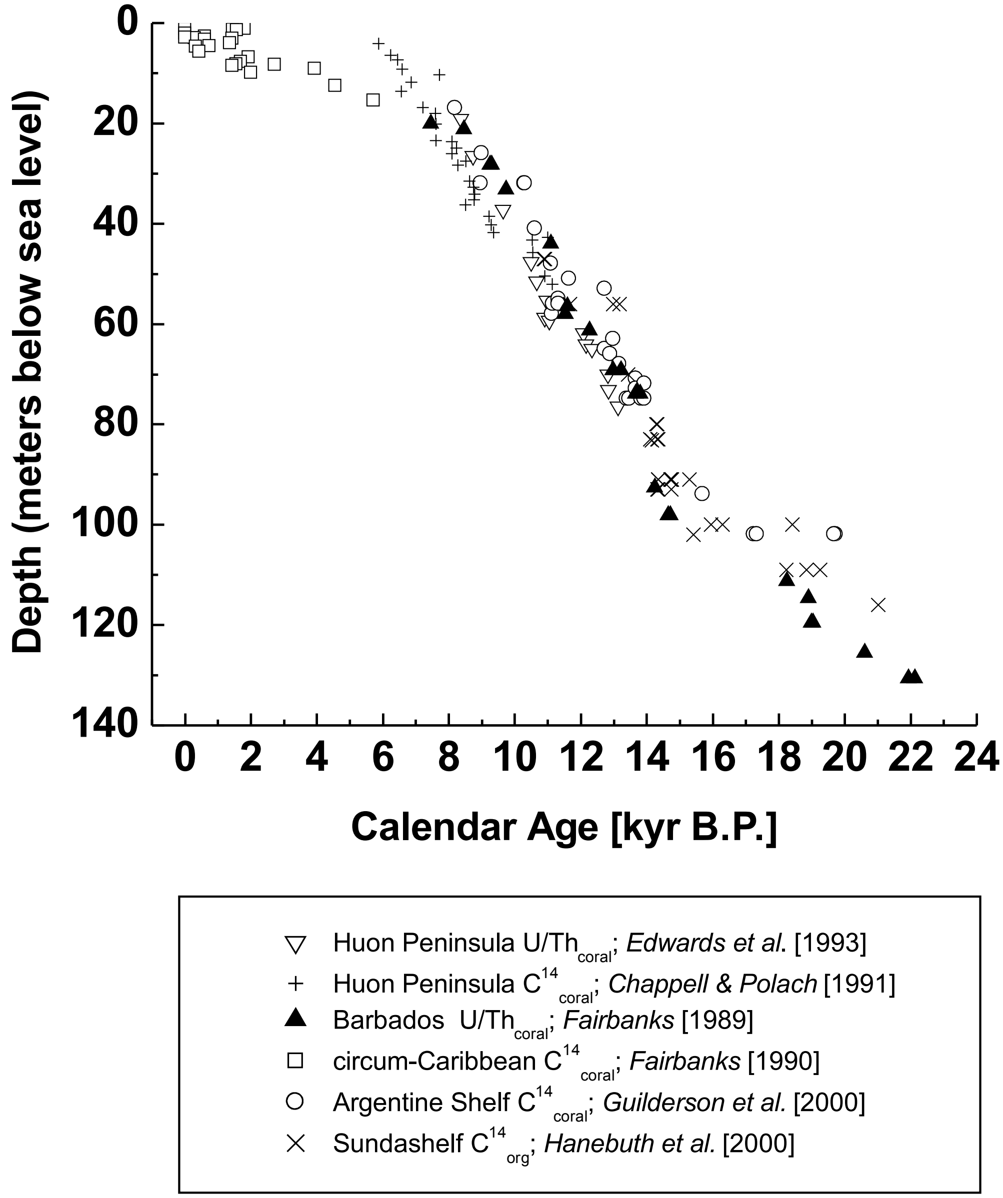

Figure 4.3: Compilation of sea-level data used to remove ice volume signal from planktonic $\delta^{18}O$ time series. All data have been corrected for their tectonic uplift and are converted into calendar ages using INTCAL98/Calib4 [*Stuiver et al.,* 1998a, b]. However U/Th ages have been used instead of ^{14}C ages if available.

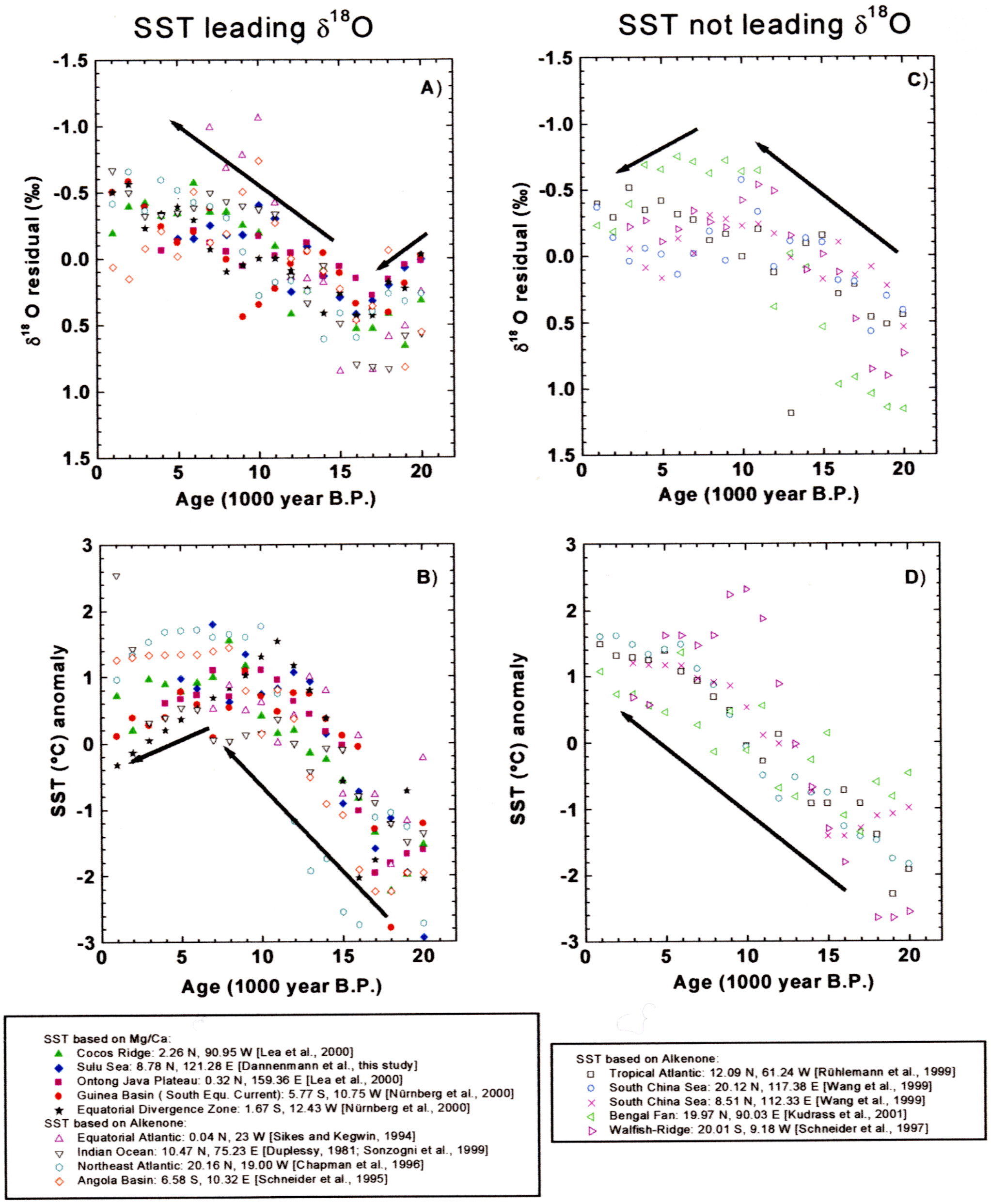

Figure 4.4: Oxygen isotope ($\delta^{18}O$) and SST data age in 1000 yrs B.P.. Ice volume change of 1.0 ‰ for glacial-interglacial range has been subtracted from the $\delta^{18}O$ record. **(A)** Compilation of $\delta^{18}O$ from cores where SST is leading $\delta^{18}O$ record. **(B)** Compilation of SST from cores where SST is leading $\delta^{18}O$. **(C)** Compilation of $\delta^{18}O$ from cores where SST is not leading $\delta^{18}O$. **(D)** Compilation of SST from cores where SST is not leading $\delta^{18}O$.

Therefore, I argue that as temperature proxies foraminiferal Mg/Ca and $\delta^{18}O_{residual}$ are independently affected by thermocline changes. This also suggests that for the purpose of reconstructing past changes in SSS, it is better to use SST estimates based on Mg/Ca rather than alkenones because both Mg/Ca and $\delta^{18}O$ are measured on the same species of foraminifera in the same sample, and thus by subtracting the $SST_{Mg/Ca}$ from the $\delta^{18}O_{residual}$ the additional temperature difference based on the calcification depths in each record will theoretically cancel each other out, and the estimate of $\delta^{18}O_{seawater}$ will be more accurate.

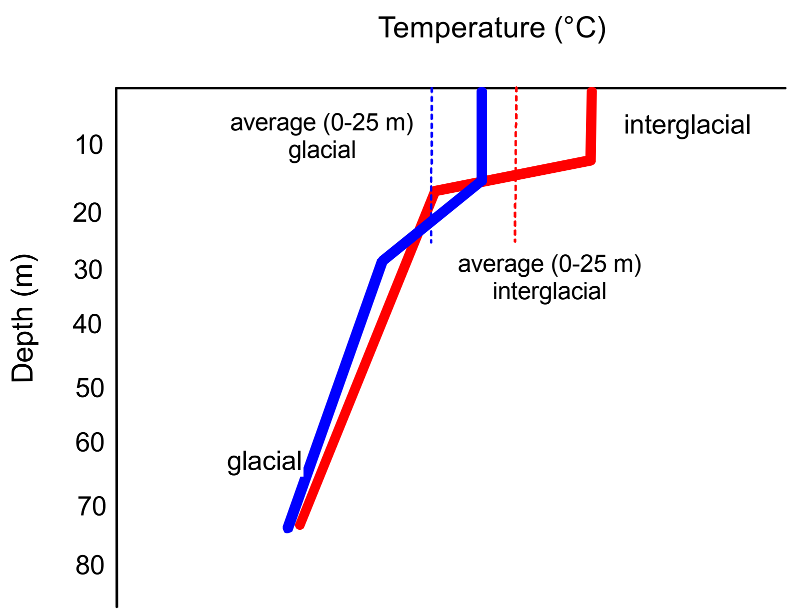

Figure 4.5: Hypothetical thermocline reconstruction for the last glacial maximum and interglacial. Vertical bars indicate average temperature change for the uppermost 25 meters.

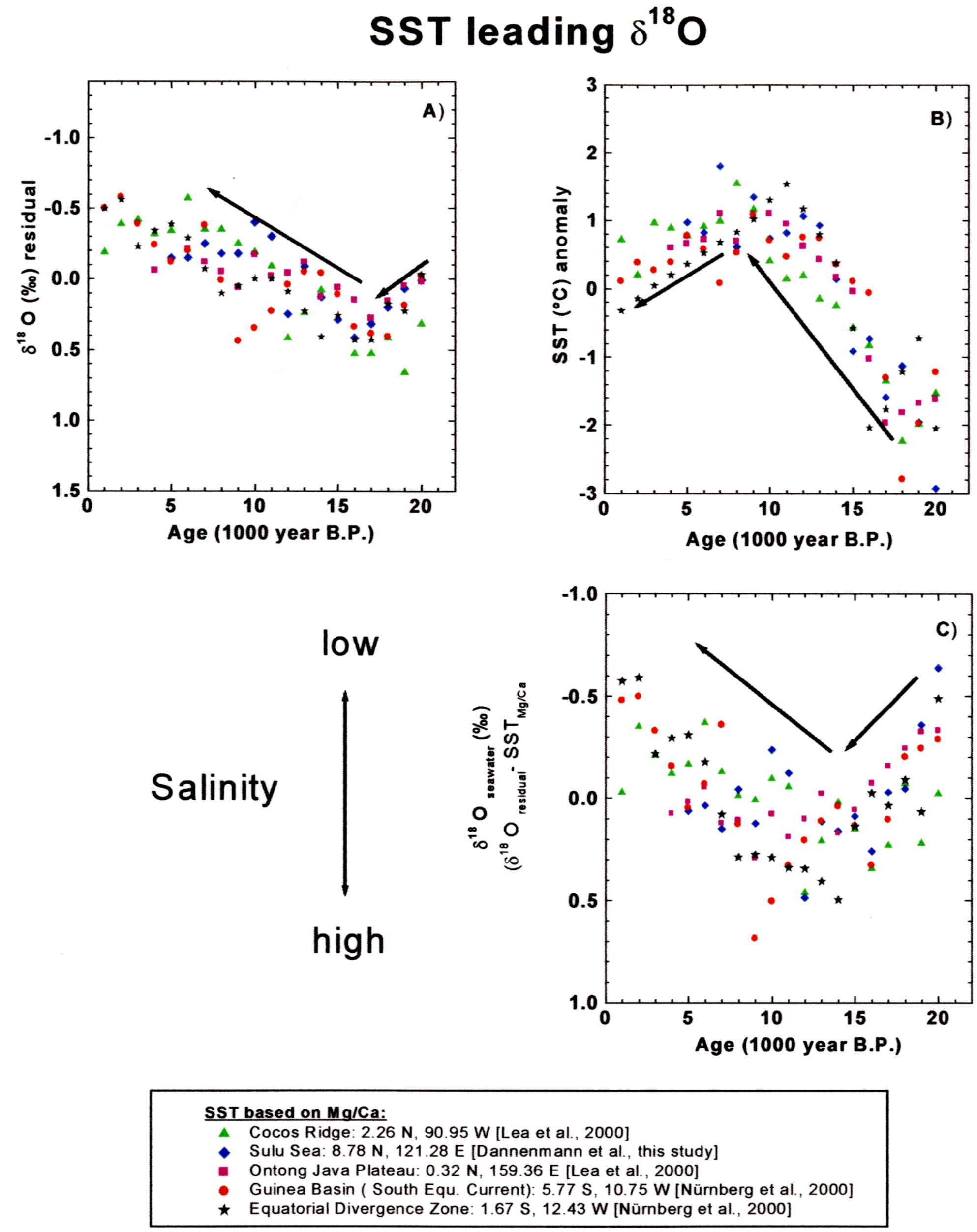

Figure 4.6: (A) Oxygen isotope ($\delta^{18}O$) and **(B)** SST data versus ages in 1000 years B.P... Sea level change of 1.0 ‰ for glacial-interglacial range has been subtracted from the $\delta^{18}O$ record ($\delta^{18}O_{residual}$). Only data of cores where SST leads $\delta^{18}O$ and is based on Mg/Ca measurements are shown. Compare with Figures 4.4A and B, respectively. However cores with SST estimates based on Alkenones are excluded. **(C)** $\delta^{18}O_{seawater}$ calculated using the equation by *Erez and Luz* [1983].

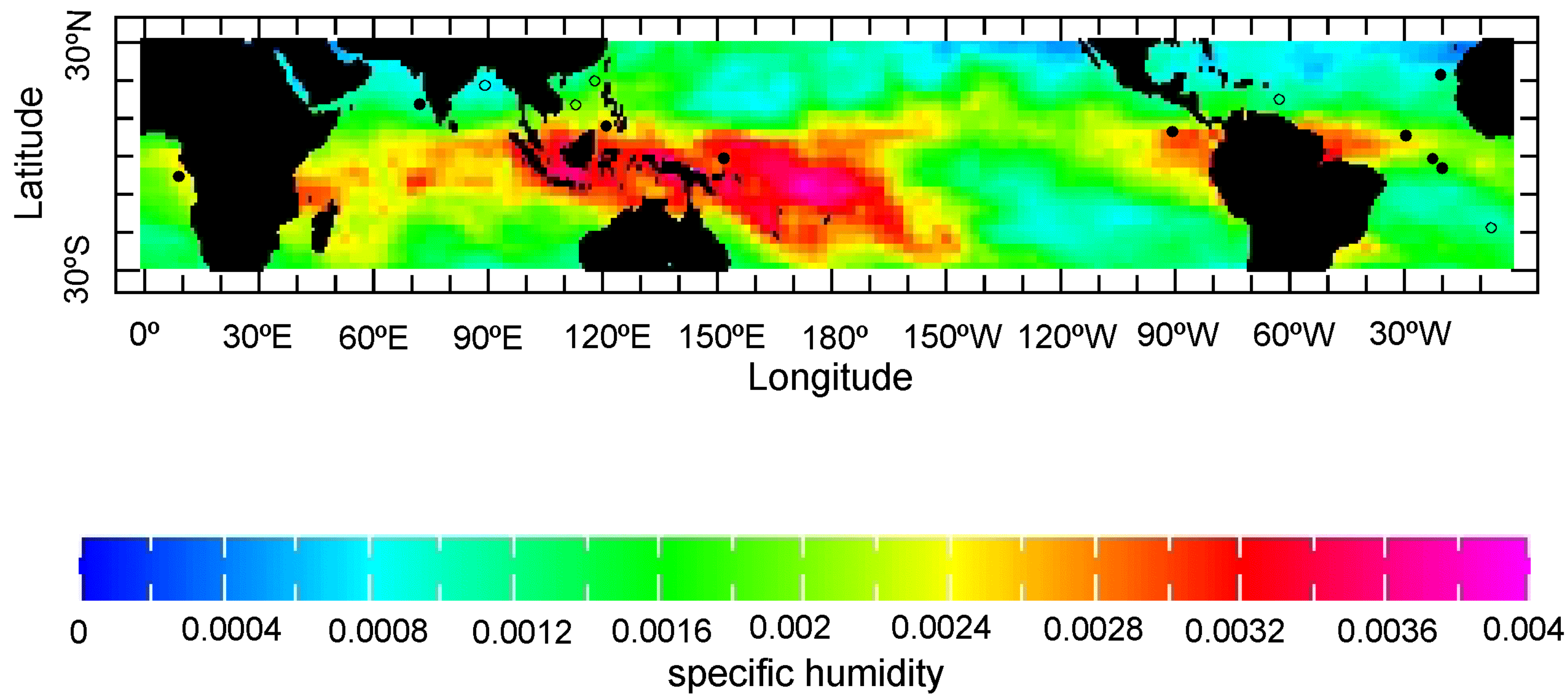

Figure 4.7: Water vapor concentration in the mid troposphere during January, 1989, a strong La Niña month. Data are taken from the European Center for Medium Range Weather Forecasts. In a La Niña year, moist air is found predominantly in the Western Pacific. Solid circles indicate SST leads the $\delta^{18}O$ record, whereas open circles indicate synchronous SST - $\delta^{18}O$ records, during the Last Glacial Maximum.

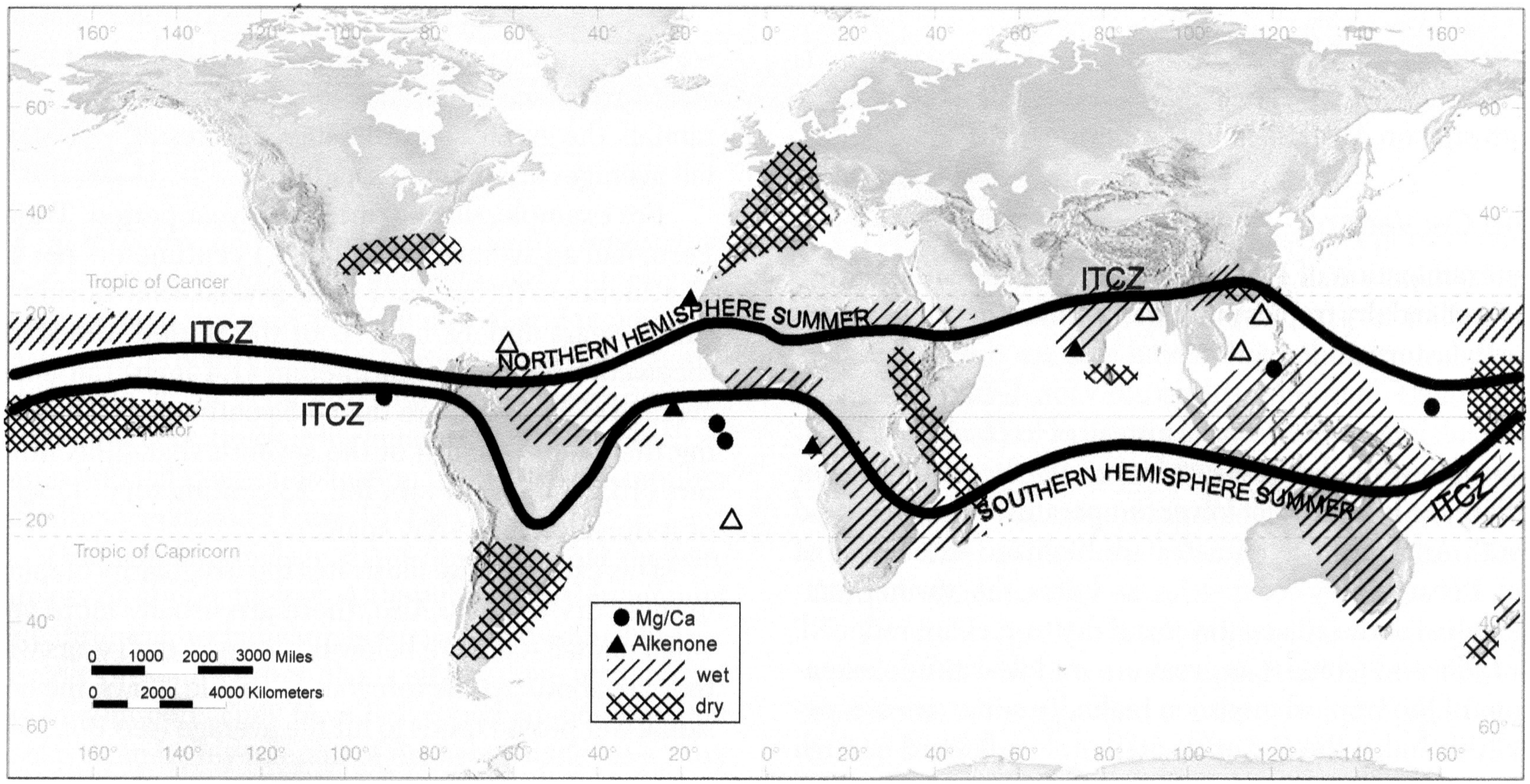

Figure 4.8: Schematics of the spatial and temporal responses of global hydro-climatological variables during a strong La Niña phase [modified from *Halbert and Ropelewski*, 1992]. Location of ocean sediment cores used to examine glacial-interglacial sea surface temperature and salinity changes by means of Mg/Ca (circle) and alkenones (triangle) analyses. Solid symbols indicate SST leads the $\delta^{18}O$ record, whereas open symbols indicate synchronous SST - $\delta^{18}O$ during the Last Glacial Maximum.